

Machine learning adaptation for laminar and turbulent flows: applications to high order discontinuous Galerkin solvers

Kenza Tlaes · Kheir-Eddine Otmani ·
Gerasimos Ntoukas · Gonzalo Rubio · Esteban
Ferrer

Received: date / Accepted: date

Abstract We present a machine learning-based mesh refinement technique for steady and unsteady flows. The clustering technique proposed by Otmani et al. [1] is used to mark the viscous and turbulent regions for the flow past a cylinder at $Re=40$ (steady laminar flow) and $Re=3900$ (unsteady turbulent flow). Within this clustered region, we increase the polynomial order to show that it is possible to obtain similar levels of accuracy to a uniformly refined mesh. The method is effective as the clustering successfully identifies the two flow regions, a viscous/turbulent dominated region (including the boundary layer and wake) and an inviscid/irrotational region (a potential flow region). The data used within this framework are generated using a high-order discontinuous Galerkin solver, allowing to locally refine the polynomial order (p -refinement) in each element of the clustered region. For the steady laminar test case we are able to reduce the computational cost up to 32% and for the unsteady turbulent case up to 33%.

Keywords Machine Learning · clustering · Navier-Stokes equations · large eddy simulation · mesh refinement · discontinuous Galerkin

1 Introduction

Within the context of computational fluid dynamics (CFD) and the modeling of complex physical phenomena, there is a continuous effort to reduce the cost of the numerical simulations while increasing the level of accuracy. One methodology along these lines, that has been used extensively across the

Kenza Tlaes , Kheir-Eddine Otmani, Gerasimos Ntoukas (E-mail: gerasimos.ntoukas@upm.es), Gonzalo Rubio and Esteban Ferrer
ETSIAE-UPM - School of Aeronautics, Universidad Politécnic de Madrid. Plaza Cardenal Cisneros 3, E-28040 Madrid, Spain. // Center for Computational Simulation, Universidad Politécnic de Madrid, Campus de Montegancedo, Boadilla del Monte, 28660, Madrid, Spain.

literature, is to use local refinement (e.g., by augmenting locally to quality of the mesh or by increasing the local polynomial order of approximation within the perspective of higher-order solvers). This allows to reduce the number of degrees of freedom and the associated simulation cost while increasing the solution accuracy, especially in particular regions of interest. This is the case for flows where viscous and turbulent regions can be clearly separated from inviscid regions. Flows belonging to this category include bluff bodies (e.g., cylinders) and aerodynamical shapes (e.g., airfoils). In these types of flow, the boundary layer and wake require local mesh refinement while the potential flow regions, away from walls and the wake, can be resolved using a coarser mesh resolution.

To perform the local refinement it is necessary to define some criteria, which will identify the location and the level of refinement required. These sensors can be classified, see [2], into three distinct categories. The feature-based indicators [3, 4, 5], the local error-based indicators [6, 7, 8] and the goal-oriented indicators [9, 10, 11]. The feature-based indicators are deduced from physical or theoretical properties of the flow, and by observation of how these influence the different aerodynamical quantities (e.g., lift, drag). These methods are deemed as inexpensive and straightforward to implement, but typically lack robustness and can be case dependent. The second group of indicators, the local error-based, identifies regions that need to be refined depending on high values of quantified error. This can be defined as the difference between the numerical and the exact solution (or an approximation of it). It requires the solution in various levels of meshes and can become relatively expensive before reaching a suitable numerical setup. The goal-oriented indicators evaluate the contribution of the error related to a specific target functional (e.g., adjoint-based), but it is costly as a new system of equations needs to be solved.

In this work, we concentrate on the first approach, the feature-based adaptation, since it constitutes a cost-effective method of locating the regions of interest and adjusting the local degrees of freedom. We propose a new robust methodology which removes some of the typical drawbacks of feature-based methods. For instance, one of the drawbacks of feature-based adaptation is the use of sensors which are related to physical quantities. An arbitrary threshold parameter is used to define the isosurface based on the feature. The isosurface defines the boundary between the regions requiring refinement and the rest of the domain. The threshold defining the isosurface is an arbitrary user-defined parameter that defines the region (or elements in the mesh) selected for refinement. Feature based adaptation typically needs an iterative trial-and-error process to define a suitable threshold parameter and to obtain convergence in the aerodynamic functionals (e.g., lift, drag). This paper employs a machine learning-based methodology to select the refinement regions while avoiding the iterative process needed to specify it.

The development of machine learning (ML) techniques during the past decade has percolated into natural sciences and engineering [12, 13, 14]. Specifically, on the topic of flow region recognition, ML and CFD have been combined using a supervised machine learning-based framework [15] to identify the flow

state (turbulent or non-turbulent flow). Different training datasets at different Reynolds numbers are used to train Extreme Gradient Boosting (XGBoost). This model can efficiently generate a robust detector for identifying turbulent regions for a flow past a circular cylinder. In the same context, a machine learning algorithm has been used in [16] to distinguish the grid cells that contain part of the boundary layer, shock waves, or external inviscid flow from RANS solutions. Within the framework of mesh adaptation, The authors of [17] introduced artificial neural networks to perform h -adaptation by predicting the desired element aspect ratio from readily accessible features of the primal and adjoint solutions. The neural network models not only reproduced the correct anisotropy for cases in the training data set, but they could also generalize to flow fields not considered during training. Yang et al. [18] proposed a work in h -refinement in which a feedforward neural network is used for adaptive mesh refinement.

In this work, we study the capabilities of the clustering technique developed in [1] as a mesh adaptation sensor. This clustering technique is capable of separating the flow into two regions, a viscous and turbulent dominated region (boundary layer and wake region) and an inviscid, irrotational region (outer flow region). The clustering technique is effective, as presented in the numerical experiments of this paper, in turbulent and laminar test cases. The Gaussian Mixture Model (GMM) model along with a feature space used in [1] is parameter free and does not require the tuning of any threshold value.

The viscous-dominated region requires a finer mesh than the inviscid region. Therefore, we propose to use a high-order polynomial approximation to solve the viscous-dominated region and a low-order polynomial approximation for the inviscid region. The aim is to accurately predict the flow features and get an equivalent solution to that of a uniform high polynomial order at a reduced cost. One advantage of having only two regions is that the computational overhead related to the mortar computation is reduced (compared to other techniques that use different polynomial orders for every element in the domain ([6, 19, 20])). Additionally, the clustering-adaptation is performed only once when the flow is developed (for steady and unsteady simulations). This simplifies the load-balancing process required for parallel computations.

The rest of this paper is organized as follows. Initially, we present the methodology in section 2, including the clustering technique and the adaptation algorithm. Then, in section 3 we present the results along with the analysis of the numerical experiments for the flow past a cylinder at $Re=40$ (steady laminar regime) and $Re=3900$ (unsteady turbulent regime) .

2 Methodology

In this section, we define the clustering technique and introduce the details of the flow invariants necessary for the cluster. Also, we present the adaptation algorithm and a brief description of the high-order solver used to carry out the simulations.

2.1 Clustering of viscous/turbulent flow region

To classify different flow regions, we use the technique proposed in [1], where the principal invariants of the strain and rotational rate tensors were used as input to the Gaussian Mixture Model (see next section) to identify the two flow regions (a viscous rotational and inviscid irrotational region). The feature space used as input to the GMM relies on Galilean invariants of the flow. The feature space is $E = \{Q_S, R_S, Q_\Omega\}$, where Q_S and R_S are the two principal invariants of the strain rate tensor S defined as

$$Q_S = \frac{1}{2} ((\text{tr}(S))^2 - \text{tr}(S^2)), \quad (1)$$

$$R_S = -\frac{1}{3} \det(S). \quad (2)$$

S is the strain rate tensor given by $S = (J + J^T)/2$ and $J = \nabla U$ is the gradient of the velocity field $U = (u, v, w)$. The first invariant of the strain rate tensor Q_S is relevant in indicating regions of high local viscous dissipation rate of the kinetic energy $\epsilon = -4\mu Q_S$ [21], where μ is the dynamic viscosity of the flow. R_S is the second strain rate tensor invariant which indicates strain production or destruction in the flow field [22]. The rotational rate tensor Ω has one invariant defined as:

$$Q_\Omega = -\frac{1}{2} (\text{tr}(\Omega^2)), \quad (3)$$

where $\Omega = (J - J^T)/2$. Q_Ω indicates rotational regions in the flow field as it is proportional to enstrophy density ξ [21]. The GMM along with the feature space E is used to detect two flow regions, a rotational viscous dominated region and an inviscid irrotational region. This methodology is applied in two different flow regimes, a laminar flow past a cylinder at $Re = 40$ and a turbulent flow past a cylinder at $Re = 3900$.

2.2 Gaussian Mixture Model(GMM)

The Gaussian Mixture Model is an unsupervised machine learning algorithm that assigns data to different cluster membership probabilities. Each point in the data will follow a certain Gaussian distribution based on a probability measure. The number of clusters must be selected before training.

The GMM considers the data as a combination of normal distributions. Each of the normal distributions is characterized by its mean and variance parameters. This model estimates these parameters by performing a maximum likelihood estimation. One of the common methods used to perform this estimate is the expectation-maximization method [23]. The expectation maximization method is an iterative process to estimate the parameters of a probability density through maximization of a likelihood function. This process is essentially done in two steps, the expectation step and the maximization step. In the expectation step, the conditional expectation of the given data

is computed after randomly initializing the parameters. In the maximization step, the likelihood of the data is maximized and then a new estimation of the parameters is given. The algorithm will repeat the expectation and maximization steps iteratively until it reaches the convergence tolerance where the expected values computed in the expectation step do not change significantly. The number of normal components (clusters) is $N = 2$ as we want to identify two distinct flow regions, a viscous/turbulent-dominated rotational region (boundary layer and wake region) and an inviscid irrotational region (outer region). This model is implemented using the Gaussian mixture class in the scikit-learn Python library [24].

2.3 Cluster based adaptation

The regions identified by the clustering technique will be used for local p -adaptation. The clustering technique will assign to each degree of freedom in the mesh two membership probabilities of belonging to the regions of interest. The probability p_c for the clustered viscous/turbulent region and p_i for the outer region. Within each element, the mean of membership probabilities $p_{c_j}|_{j=1}^N, p_{i_j}|_{j=1}^N$ for each region is computed as follows,

$$\bar{p}_v = \frac{1}{N} \sum_{j=1}^N p_{c_j}, \quad p_{c_j} \in [0, 1], \quad (4)$$

$$\bar{p}_i = \frac{1}{N} \sum_{j=1}^N p_{i_j}, \quad p_{i_j} \in [0, 1], \quad (5)$$

where $N = (P + 1)^3$ is the number of degrees of freedom of each element of the mesh, and P denotes the polynomial order associated to the high order discretization. An element will be assigned to the region with the highest mean of membership probabilities $\bar{p} = \max(\bar{p}_i, \bar{p}_v)$. The same process will be applied for all elements to supply each one with a region ID, viscous/turbulent or inviscid. Having marked the elements belonging to each region, we can now modify the polynomial order in each region accordingly.

The cluster based adaptation involves three steps. In the first step we run a simulation with a polynomial order, $P = P_{cluster}$, until the flow is fully developed. $P_{cluster}$ is chosen so that the solver captures, with the desired level of accuracy, all the features of the flow. In the second step we perform the clustering, as explained in the previous paragraph. In the third step, we use the ID of each element, depending on which region it belongs to, and assign the corresponding polynomial order within that element. In the present work, we coarsen the polynomial in the inviscid regions, $P_{inviscid}$, while keeping the original high-order polynomial, $P_{cluster}$, in the elements belonging to the viscous/turbulent region. It is reasonable to keep $P_{cluster}$ in the viscous region, as it was selected

to achieve a certain level of accuracy. However this high resolution can be relaxed using $P_{inviscid} < P_{cluster}$ in the inviscid region, that presents a lower flow complexity. However, different strategies to perform adaptation based on this clustering may be proposed (e.g., h -refinement/coarsening). Finally, the simulation is restarted with the adapted polynomial order from the same instant until we reach the final solution. This process is summarized in algorithm 1.

Algorithm 1 Methodology algorithm

```

Start the simulation using uniform polynomial order  $P_{cluster}$ 
Stop the simulation when the flow is fully developed
Train GMM with feature space  $E$ 
Return  $p_c$  and  $p_i$  ▷ Membership probabilities for every point
for  $k$  in number of elements do
   $\bar{p}_i = \frac{1}{N} \sum_{j=1}^N p_{i_j}$ 
   $\bar{p}_v = \frac{1}{N} \sum_{j=1}^N p_{c_j}$ 
  if  $\bar{p}_v \geq \bar{p}_i$  then
     $P(k) \leftarrow P_{cluster}$  ▷ high-order polynomial in the viscous rotational region
  else if  $\bar{p}_v < \bar{p}_i$  then
     $P(k) \leftarrow P_{inviscid}$  ▷ low-order polynomial in the inviscid irrotational region
  end if
end for
Return  $P$ 
Restart the simulation using  $P$ 

```

2.4 High order discontinuous Galerkin solver

The data used in this work have been generated using the high-order spectral element CFD solver HORSES3D [25]. HORSES3D is a 3D parallel code developed at ETSIAE-UPM (the School of Aeronautics of the Polytechnic University of Madrid). This framework uses the high-order discontinuous Galerkin spectral element method (DGSEM) and is written in modern Fortran 2003. It targets simulations of fluid-flow phenomena such as those governed by compressible and incompressible Navier-Stokes equations, and it supports curvilinear hexahedral meshes of arbitrary order. There are several options of subgrid turbulence models for the users to choose from for LES simulations such as the Smagorinsky subgrid model, Wale and Vreman. One of the main features offered in HORSES3D is its support for anisotropic p -non-conforming elements, as the polynomial order can be varied independently in each element in each direction. In this work, we make use of the adaptation capability to increase/decrease the polynomial order uniformly within each element in the regions determined by the clustering technique.

3 Results and Discussion

The mesh refinement strategy is applied to a steady flow test case around a cylinder at $Re=40$ and an unsteady turbulent flow around a circular cylinder at $Re=3900$, with a Smagorinsky subgrid closure model.

3.1 Flow past a cylinder at $Re=40$

In this test case, we refine the mesh for steady laminar flow around a cylinder at $Re=40$. The steady flow data are generated in a mesh of 684 elements with 85500 degrees of freedom using a uniform polynomial order $P = 4$. The adaptation is carried out following the procedure described in algorithm (1). Figure (1a) shows the regions identified using the clustering GMM model. The initial, high polynomial order is kept in the selected elements in figure (1b) based on the mean of probabilities to belong to the viscous rotational region. For this numerical experiment we use $P_{cluster} = 4$ for the viscous regions and $P_{inviscid} \in [1, 2, 3]$ for the inviscid ones.

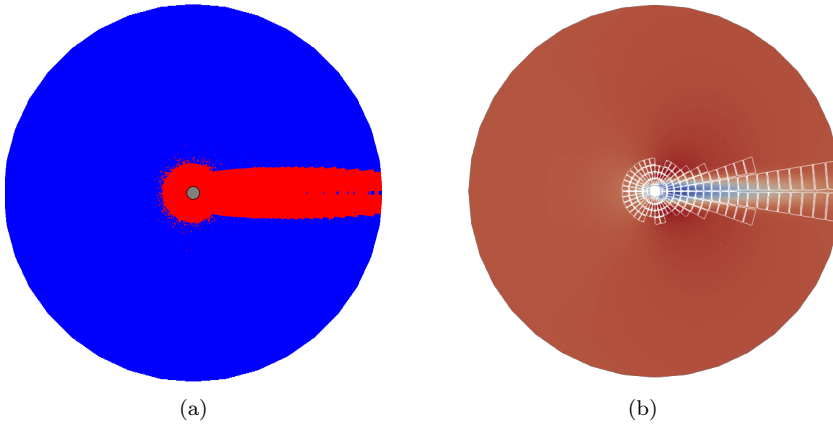


Fig. 1: Regions detected with the GMM along with the feature space E for flow past a cylinder at $Re = 40$. **Red**: viscous rotational region. **Blue**: outer region (1a), selected elements for high-order polynomial refinement (1b) for the flow past a circular cylinder at $Re = 40$

We run all simulations until the maximum residuals decreases by a factor of 1000. At this point the flow is not converged yet, but the wake has developed. We can use this data to perform the clustering and detect the regions that need adaptation/coarsening. Having adapted, we converge the simulation until the maximum residual is 10^{-4} . This adapt and converge technique reduces significantly the computational time. Figure 2 shows the convergence history of the homogeneous $P = 4$ solution and the clustering adapted solution ($P_{cluster} = 4$

and $P_{inviscid} \in [1, 2, 3]$), where it can be observed that convergence is accelerated when adaptation is performed. The computational savings and the corresponding degrees of freedom for each simulation are presented in table I. The adapted solutions for $P_{inviscid} \in [1, 2, 3]$ exhibit 32%, 29% and 19% reduction of computational time accordingly compared to the homogeneous ($P = 4$) solution and 67%, 55% and 35% less degrees of freedom.

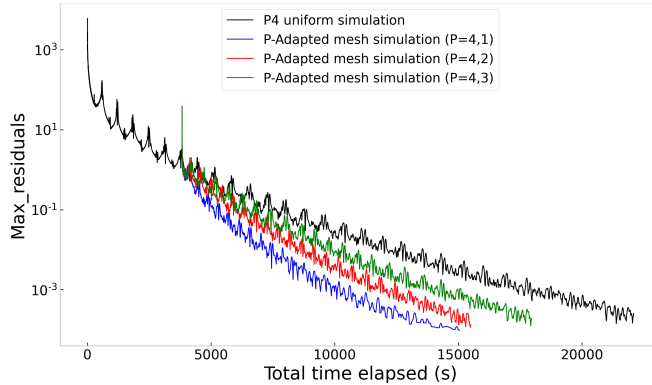


Fig. 2: Max residuals for homogeneous and P -adapted solutions

Table I: Results shown for residuals = 10^{-4} (converged solution).

$P_{cluster}$	$P_{inviscid}$	Adapted	computational time(s)	C_d	DoF
2	2	No	8.39×10^3	1.5062	18 468
3	3	No	1.23×10^4	1.5264	43 776
4	4	No	2.21×10^4	1.5221	85 500
4	1	Yes	1.50×10^4	1.5214	27 936
4	2	Yes	1.58×10^4	1.5225	38 460
4	3	Yes	1.79×10^4	1.5222	55 488

Finally, table II reports drag values extracted from the literature. Comparing tables II and I, we observe that the baseline homogeneous (for $P=4$) and all clustered adapted solutions ($P_{cluster} = 4$ and $P_{inviscid} \in [1, 2, 3]$) provide accurate predictions for the drag coefficient.

This first laminar steady case shows that the GMM clustering can separate the viscous region (the boundary layer and wake) from the outer inviscid. Refinement of the clustered region and coarsening of the inviscid outer region shows that the detected clustered region is indeed responsible for errors in drag, and that refining it increases the accuracy of the simulations. In addition,

Table II: Comparison of the results for the drag coefficient (C_d) for flow past a cylinder at $Re=40$

Case	C_d
Dennis and Chang [26]	1.52
Fornberg [27]	1.50
Choi et al. [28]	1.49

we conclude that the clustering adaptation is an efficient technique for mesh adaptation in steady flows and can help to speed up convergence.

3.2 Flow past a cylinder at $Re=3900$

This case has been considered extensively by numerous researchers within the numerical [29, 30] and experimental spectrum [29, 31, 32]. For this case we use a 2^{nd} order mesh of 20736 hexahedral elements. The mesh has been extruded in the spanwise direction as $L_z/D = \pi$ and subdivided into 16 elements along this direction. The solution has been calculated using a uniform polynomial order of $P \in [3, 4]$, as well as an adapted solution defined with the clustering algorithm with $P_{cluster} = 4$ and $P_{inviscid} = 2$. In this turbulent case, using $P_{inviscid} = 1$ resulted in diverging simulations probably due to aliasing instabilities at the interface between elements with different polynomial orders (mortar surfaces), for this reason we only report results for $P_{inviscid} = 2$. The adaptation has been performed using the clustering algorithm on a single instant of the flow field after the wake has developed. The adapted mesh is presented in figure 3a. A constant non-dimensional time step of $\Delta t = 2 \times 10^{-3}$ has been used throughout all the different simulations. To minimize the aliasing errors and ensure that the method is robust, a split form discretization has been employed with Pirozzoli averaging [33].

To measure statistical quantities, we follow [29] and allow the flow to develop for a time interval of $t = 150D/U_c$ to remove the influence of the initial condition. Then the statistics are gathered for a time duration of approximately 100 shedding cycles for each of the simulations carried out, which is in line with the averaging intervals in the literature [29].

The results for the mean drag coefficient C_d , Strouhal number St and the recirculation length L_r are presented in table III. We compare the results obtained from HORSES3D with uniform $P = 3$, $P = 4$ solutions and a p-adapted mesh against numerical and experimental results from previous works. As presented, the uniform $P = 4$ and the adapted results fall well within what is reported in the literature. For the uniform $P = 3$ solution, we observe that the mean drag value is severely under-predicted due to the lack of sufficient resolution, even though the Strouhal number is close to the reported values.

The clustering algorithm is able to successfully track the region of interest and through local p -refinement we attain a solution with 41% less degrees

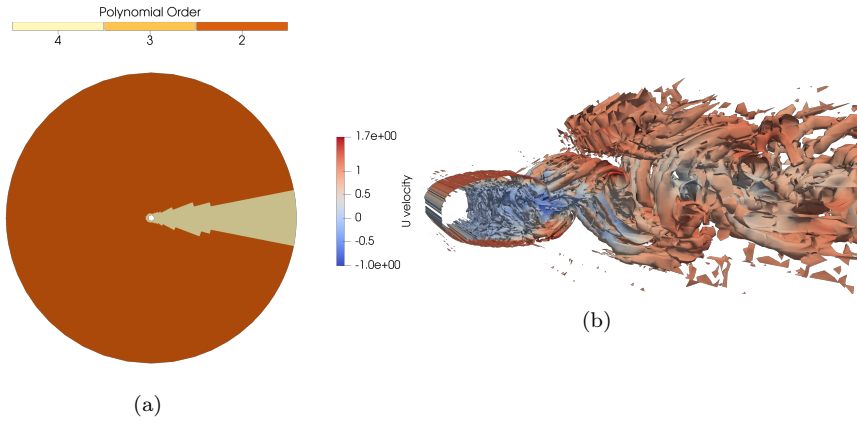


Fig. 3: Polynomial order distribution from the clustering algorithm for the cylinder at $Re=3900$ test case presented in 3a. 3b presents an isosurface of the $Q_{crit} = 0.1$ coloured with the axial velocity u

Table III: Comparison of the mean statistical quantities for the cylinder at $Re = 3900$ HORSES3D and the literature. We compare the Strouhal number St , the drag coefficient C_d and the recirculation length L_r . All simulations used a spanwise length $L_z/D = \pi$

	St	C_d	L_r	$L_z \setminus D$
Uniform P3	0.202	0.7844	1.36	π
Uniform P4	0.203	0.9513	1.64	π
Cluster-Adapt P4-P2	0.204	0.9506	1.63	π
Parnadeau et al. [29]	0.208	-	1.56	π
Snyder and Degrez [34]	0.207	1.09	1.30	π
Kravchenko and Moin [35]	0.210	1.04	1.35	π
Breuer [36]	-	1.07	1.20	π
Franke and Frank [37]	0.209	0.98	1.64	π
(DNS) Ma et al. [30]	0.219	1.59	-	π
Ouvrard et al. [38]	0.223	0.94	1.56	π

of freedom, for a similar level of accuracy, compared to the uniform $P = 4$ solution, as presented in table IV. The adapted solution has only 16% more degrees of freedom than the uniform $P = 3$ solution but offers superior results as presented in table III and figure 4. In terms of computational cost, as presented in table IV, the adapted solution is 33% faster than the reference uniform $P = 4$ solution for any given simulation interval.

The statistics for this test case are presented in figure 4. The results of this work are compared against the experimental (PIV) and numerical results (LES) presented in [29]. In figure 4a the results of the variance of the streamwise fluctuations for three different positions $x/D = [1.06, 1.54, 2.02]$ are presented. The adapted and uniform $P = 4$ results are in good agreement with the PIV and LES data. It should be noted that in the position $x/D = 1.06$ the

Table IV: Comparison of the mean statistical quantities for the cylinder at Re=3900 results from HORSES3D and the literature

	DoFs	reduction of DoFs	reduction of comp. time
Uniform P4	2.60M	-	-
Uniform P3	1.33M	49%	50%
Cluster-Adapt P4-P2	1.55M	41%	33%

two strong peaks, due to the transitional state of the shear layer [29], are lower for the uniform $P = 3$ case which can be attributed to the lack of proper resolution [29]. In figure 4b we present the covariance of the fluctuations. In this case, we also have good agreement between the reference data and the adapted and uniform $P = 4$ solution. The uniform $P = 3$ solution deviates, indicating that this level of resolution is not sufficient to capture the correct phenomena. The differences are less pronounced in the results presented in figures 4d, 4e as we observe a good agreement for the mean streamwise and normal velocities between the reference results (LES, PIV) and the results of this work. The variance of the normal velocity fluctuations in figure 4f is in good agreement, although the uniform $P = 3$, $P = 4$ and clustering p-adaptation results of this work underestimate the peak along the position $x/D = 2.02$. Lastly, the mean streamwise velocity along the centerline, presented in figure 4c, is close to the reference data but we observe that the point of minimum velocity is over-predicted in the results from HORSES3D.

This second turbulent case shows that the clustering adaption can be very useful for turbulent unsteady cases. The GMM clustering is able to mark viscous and turbulent regions in the boundary layer and wake, where higher resolution is required and separate it from the outer inviscid region, where a lower resolution can be used.

4 Conclusion

The presented methodology has been successfully applied and resulted in accelerating the fluid flow simulation around a circular cylinder at Reynolds 40 (steady laminar regime) and Re=3900 (unsteady turbulent regime) while maintaining the expected levels of accuracy. The local adaptation strategy decouples the viscous/turbulent region from the outer inviscid regions and through mesh refinement/coarsening it achieves comparable results to those with uniformly refined meshes. For the laminar case, we have shown that the p -adapted solution with polynomial orders ($P_{cluster} = 4, P_{inviscid} = [1, 2, 3]$) has the same accuracy as the homogeneous solution with a uniform polynomial order ($P = 4$) while showing 67%, 55% and 35% reduction in number of degrees of freedom and 32%, 29% and 19% reduction of computational time, respectively.

Furthermore, we have shown that this method is applicable to more complex unsteady turbulent flows such as that past a circular cylinder at Re=3900.

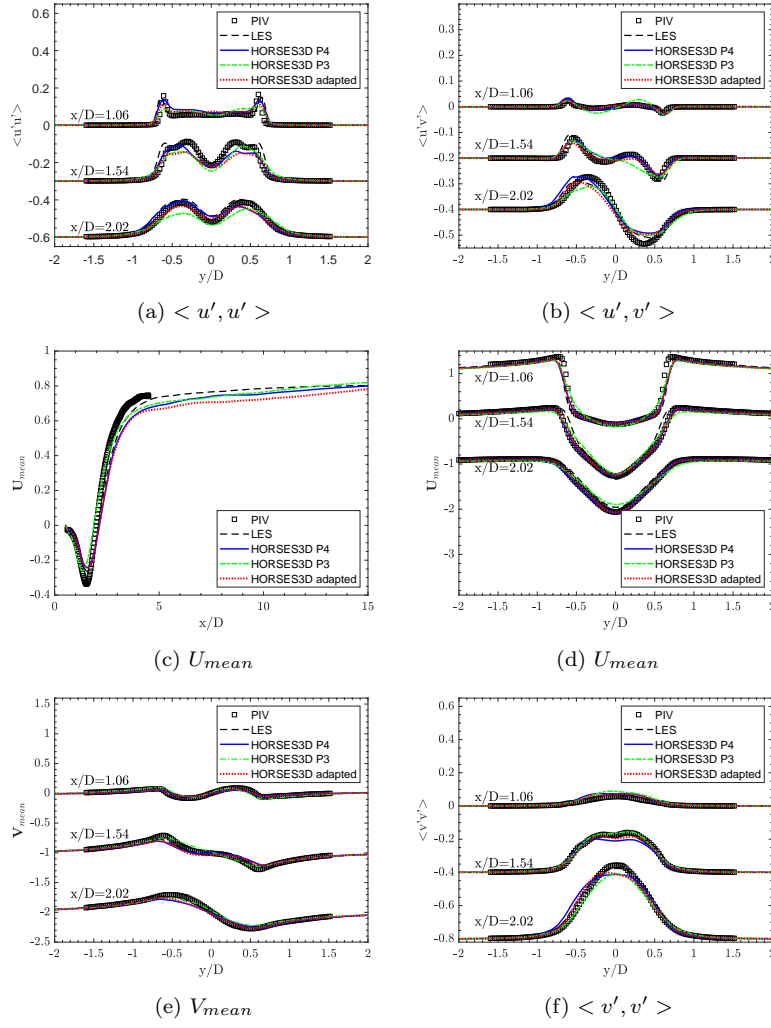


Fig. 4: Statistical quantities of the wake for the unsteady turbulent case of a flow past a cylinder at $Re=3900$. Comparison of experimental (PIV) and high resolution numerical (LES) results from [29] against uniform and adapted results from HORSES3D

The adapted solution through the clustering method is similar to the benchmark uniform solution ($P = 4$), as well as the experimental and numerical results reported in the literature, while having 41% less degrees of freedom and 33% reduced computational cost. This showcases that the algorithm tracks the regions of interest that need to be well resolved while allowing us to reduce the computational cost.

We conclude that the clustering-based adaptation is a useful tool within the feature-based methods and overcomes some of the classic drawbacks present in feature-based approaches. For example, the presented methodology does not require any threshold or iterative adaptation process to determine the refinement regions.

Acknowledgments

Gerasimos Ntoukas and Esteban Ferrer acknowledge the financial support of the European Union's Horizon 2020 research and innovation programme under the Marie Skłodowska-Curie grant agreement (MSCA ITN-EID-GA ASIMIA No 813605). Gonzalo Rubio acknowledges the funding received by the Grant SIMOPAIR (Project No. RTI2018-097075-B-I00) funded by MCIN/AEI/10.13039/501100011033 and by ERDF A way of making Europe. Esteban Ferrer would like to thank the support of the Spanish Ministry MCIN/AEI/10.13039/501100011033 and the European Union NextGenerationEU/PRTR for the grant "Europa Investigación 2020" EIN2020-112255, and also the Comunidad de Madrid through the call Research Grants for Young Investigators from the Universidad Politécnica de Madrid. Finally, all authors gratefully acknowledge the Universidad Politécnica de Madrid (www.upm.es) for providing computing resources on Magerit Supercomputer.

Data availability

The data that support the findings of this study are available from the corresponding author upon reasonable request.

References

1. Kheir-Eddine Otmani, Gerasimos Ntoukas, and Esteban Ferrer. Towards a robust detection of viscous and turbulent flow regions using unsupervised machine learning, July 2022.
2. Fabio Naddei, Marta de la Llave Plata, Vincent Couaillier, and Frédéric Coquel. A comparison of refinement indicators for p-adaptive simulations of steady and unsteady flows using discontinuous Galerkin methods. *Journal of Computational Physics*, 376:508–533, January 2019. ISSN 0021-9991.
3. Gerasimos Ntoukas, Juan Manzanero, Gonzalo Rubio, Eusebio Valero, and Esteban Ferrer. A free-energy stable p-adaptive nodal discontinuous galerkin for the cahn-hilliard equation. *Journal of Computational Physics*, 442:110409, 2021.
4. Gerasimos Ntoukas, Juan Manzanero, Gonzalo Rubio, Eusebio Valero, and Esteban Ferrer. An entropy-stable p-adaptive nodal discontinuous

- galerkin for the coupled navier–stokes/cahn–hilliard system. *Journal of Computational Physics*, 458:111093, 2022.
5. Weizhao Li, Hong Luo, Aditya Pandare, and Jozsef Bakosi. A p-adaptive discontinuous galerkin method for compressible flows using charm++. In *AIAA Scitech 2020 forum*, page 1565, 2020.
 6. Andrés M Rueda-Ramírez, Juan Manzanero, Esteban Ferrer, Gonzalo Rubio, and Eusebio Valero. A p-multigrid strategy with anisotropic p-adaptation based on truncation errors for high-order discontinuous galerkin methods. *Journal of Computational Physics*, 378:209–233, 2019.
 7. Marta de la Llave Plata, Fabio Naddei, and Vincent Couaillier. Les of the flow past a circular cylinder using a multiscale discontinuous galerkin method. In *5th International conference on Turbulence and Interactions, TI 2018*, 2018.
 8. Francesca Basile, Jean-Baptiste Chapelier, Marta de la Llave Plata, Romain Laraufie, and Pascal Frey. Unstructured h-and hp-adaptive strategies for discontinuous galerkin methods based on a posteriori error estimation for compressible flows. *Computers & Fluids*, 233:105245, 2022.
 9. Wojciech Laskowski, Gonzalo Rubio, Eusebio Valero, and Esteban Ferrer. A functional oriented truncation error adaptation method. *J. Comput. Phys.*, 451:110883, 2022.
 10. Richard P Dwight. Goal-oriented mesh adaptation for finite volume methods using a dissipation-based error indicator. *International journal for numerical methods in fluids*, 56(8):1193–1200, 2008.
 11. Nicholas Burgess and Dimitri Mavriplis. An hp-adaptive discontinuous galerkin solver for aerodynamic flows on mixed-element meshes. In *49th AIAA Aerospace Sciences Meeting including the New Horizons Forum and Aerospace Exposition*, page 490, 2011.
 12. Steven L. Brunton and J. Nathan Kutz. *Data-Driven Science and Engineering: Machine Learning, Dynamical Systems, and Control*. Cambridge University Press, 2019.
 13. Paul Garnier, Jonathan Viquerat, Jean Rabault, Aurélien Larcher, Alexander Kuhnle, and Elie Hachem. A review on deep reinforcement learning for fluid mechanics. *Computers & Fluids*, 225:104973, 2021. ISSN 0045-7930.
 14. Ricardo Vinuesa and Steven L Brunton. Enhancing computational fluid dynamics with machine learning. *Nature Computational Science*, 2(6):358–366, 2022.
 15. Binglin Li, Zixuan Yang, Xing Zhang, Guowei He, Bing-Qing Deng, and Lian Shen. Using machine learning to detect the turbulent region in flow past a circular cylinder. *Journal of Fluid Mechanics*, 905, December 2020. ISSN 0022-1120, 1469-7645. doi: 10.1017/jfm.2020.725.
 16. Ettore Saetta and Renato Tognaccini. Identification of flow field regions by Machine Learning. In *AIAA SCITECH Forum*. American Institute of Aeronautics and Astronautics, 2022.
 17. Krzysztof J. Fidkowski and Guodong Chen. Metric-based, goal-oriented mesh adaptation using machine learning. *Journal of Computational*

- Physics*, 426:109957, February 2021. ISSN 00219991.
18. Jiachen Yang, Tarik Dzanic, Brenden Petersen, Jun Kudo, Ketan Mittal, Vladimir Tomov, Jean-Sylvain Camier, Tuo Zhao, Hongyuan Zha, Tzanio Kolev, Robert Anderson, and Daniel Faissol. Reinforcement Learning for Adaptive Mesh Refinement. *arXiv:2103.01342 [cs, math]*, March 2021. Comment: 14 pages, 13 figures.
 19. Moritz Kompenhans, Gonzalo Rubio, Esteban Ferrer, and Eusebio Valero. Adaptation strategies for high order discontinuous galerkin methods based on tau-estimation. *Journal of Computational Physics*, 306:216–236, 2016.
 20. Moritz Kompenhans, Gonzalo Rubio, Esteban Ferrer, and Eusebio Valero. Comparisons of p-adaptation strategies based on truncation- and discretisation-errors for high order discontinuous Galerkin methods. *Computers & Fluids*, 139:36–46, November 2016. ISSN 0045-7930. doi: 10.1016/j.compfluid.2016.03.026.
 21. Yi Zhou, Koji Nagata, Yasuhiko Sakai, Yasumasa Ito, and Toshiyuki Hayase. On the evolution of the invariants of the velocity gradient tensor in single-square-grid-generated turbulence. *Physics of Fluids*, 27:075107, 2015.
 22. Carlos B. da Silva and José C. F. Pereira. Invariants of the velocity-gradient, rate-of-strain, and rate-of-rotation tensors across the turbulent/nonturbulent interface in jets. *Physics of Fluids*, 20(5):055101, 2008.
 23. A. P. Dempster, N. M. Laird, and D. B. Rubin. Maximum likelihood from incomplete data via the em algorithm. *Journal of the Royal Statistical Society: Series B (Methodological)*, 39(1):1–22, 1977.
 24. Fabian Pedregosa, G. Varoquaux, Alexandre Gramfort, V. Michel, B. Thirion, O. Grisel, Mathieu Blondel, Gilles Louppe, P. Prettenhofer, Ron Weiss, Ron J. Weiss, J. Vanderplas, Alexandre Passos, D. Cournapeau, M. Brucher, M. Perrot, and E. Duchesnay. Scikit-learn: Machine Learning in Python, 2011.
 25. E. Ferrer, G. Rubio, G. Ntoukas, W. Laskowski, O. A. Mariño, S. Colombo, A. Mateo-Gabín, F. Manrique de Lara, D. Huergo, J. Manzanero, A. M. Rueda-Ramírez, D. A. Kopriva, and E. Valero. Horses3d: a high-order discontinuous galerkin solver for flow simulations and multi-physics applications, 2022. URL <https://arxiv.org/abs/2206.09733>.
 26. SCR Dennis and Gau-Zu Chang. Numerical solutions for steady flow past a circular cylinder at reynolds numbers up to 100. *Journal of Fluid Mechanics*, 42(3):471–489, 1970.
 27. Bengt Fornberg. A numerical study of steady viscous flow past a circular cylinder. *Journal of Fluid Mechanics*, 98(4):819–855, 1980.
 28. Jung-Il Choi, Roshan C. Oberoi, Jack R. Edwards, and Jacky A. Rosati. An immersed boundary method for complex incompressible flows. *Journal of Computational Physics*, 224(2):757–784, 2007. ISSN 0021-9991.
 29. Philippe Parnaudeau, Johan Carlier, Dominique Heitz, and Eric Lamballais. Experimental and numerical studies of the flow over a circular cylinder at reynolds number 3900. *Physics of Fluids*, 20(8):085101, 2008.

30. X Ma, G-S Karamanos, and GE Karniadakis. Dynamics and low-dimensionality of a turbulent near wake. *Journal of fluid mechanics*, 410: 29–65, 2000.
31. C Norberg. Effects of reynolds number and low-intensity free stream turbulence on the flow around a circular cylinder. *Chalmers University of Technology, Department of Applied Thermoscience and Fluid Mechanics, Gothenburg, Sweden, Pub*, 2(87), 1987.
32. LM Lourenco. Characteristics of the plate turbulent near wake of a circular cylinder. a particle image velocimetry study. *In Unpublished, results taken from Beaudan and Moin*, 1994.
33. Sergio Pirozzoli. Generalized conservative approximations of split convective derivative operators. *Journal of Computational Physics*, 229(19): 7180–7190, 2010.
34. Deryl O Snyder and Gérard Degrez. Large-eddy simulation with complex 2-d geometries using a parallel finite-element/spectral algorithm. *International journal for numerical methods in fluids*, 41(10):1119–1135, 2003.
35. Arthur G Kravchenko and Parviz Moin. Numerical studies of flow over a circular cylinder at $re_d = 3900$. *Physics of fluids*, 12(2):403–417, 2000.
36. Michael Breuer. Large eddy simulation of the subcritical flow past a circular cylinder: numerical and modeling aspects. *International journal for numerical methods in fluids*, 28(9):1281–1302, 1998.
37. J Franke and W Frank. Large eddy simulation of the flow past a circular cylinder at $re_d = 3900$. *Journal of wind engineering and industrial aerodynamics*, 90(10):1191–1206, 2002.
38. Hilde Ouvrard, Bruno Koobus, Alain Dervieux, and Maria Vittoria Salvetti. Classical and variational multiscale les of the flow around a circular cylinder on unstructured grids. *Computers & Fluids*, 39(7):1083–1094, 2010.